

Scattering and Absorption in Soft X-ray Selected AGN: An Optical Polarization Survey

D. Grupe^{1,2,*}, Beverley J. Wills¹, D. Wills¹, and K. Beuermann²

¹ Department of Astronomy & McDonald Observatory, University of Texas at Austin, RLM 15.308, Austin, TX 78712, U.S.A.

² Universitäts-Sternwarte, Geismarlandstr. 11, D-37083 Göttingen, Germany

Received 20.08.1997; accepted 17.10.1997

Abstract. We have surveyed the optical linear polarization of a completely identified sample of 43 bright soft-X-ray-selected ROSAT AGN. Most (40) of these AGN show low polarization ($\lesssim 1\%$), and no clear optical reddening. This supports the suggestion from rapid X-ray variability, disk-like spectral energy distributions, and lack of cold X-ray absorption, that we are viewing a bare AGN disk. IRAS F12397+3333 and IRAS 13349+2438 show high polarization increasing to the UV – clear evidence for scattering. As well as steep, soft-X-ray spectra, they show optical reddening and rapid X-ray variability, but almost no cold X-ray absorption – a combination that suggests dusty ionized gas along the line-of-sight. Brandt et al. suggested and found these ‘warm absorbers’ for IRAS 13349+2438. IRAS F12397+3333 is a new candidate. Combining our data with the optical and X-ray spectra of the high polarization narrow-line Seyfert 1 nuclei (NLSy1s) investigated by Goodrich reveals strong correlations among optical reddening indicators (α_{opt} and $H\alpha/H\beta$), $[O\ III]/H\beta_b$, and cold intrinsic X-ray absorption ΔN_H . Optical reddening underpredicts the cold X-ray absorption, suggesting dusty warm absorbers in all the highly polarized AGN. The existence of these scattering-polarized and reddened NLSy1s suggests an orientation Unified Scheme within the class of NLSy1s, analogous to that linking Seyfert 1 and Seyfert 2 nuclei.

For some highly polarized and optically selected AGN we present new analysis of archival X-ray data, and for the highly polarized AGN new optical spectroscopy is presented in an appendix.

Key words: Polarization – Galaxies: active – Galaxies: nuclei of – Galaxies: Seyfert

1. Introduction

A popular idea among astronomers is that all AGN are powered by the same kind of engine: accretion of matter through an accretion disk onto a super-massive black hole. This idea receives strong support from high, Keplerian velocities of gas in the centers of active galaxies, and alignment of the axes of these gaseous disks with powerful radio jets. Understanding of the basic fueling mechanism remains elusive, but there may be new clues, related to the classic energy-budget problem and the so-called First Principal Component, both linking the ionizing continuum and the emission-line regions:

(a) The energy budget problem is that there appears to be insufficient ionizing continuum photons to power the broad emission lines, especially the strong, blended Fe II lines (e.g. Netzer 1985; Collin-Souffrin et al. 1988). Solutions may be that the Fe II arises from a different region, excited not by photoionization but by mechanical heating of the gas (e.g. Norman & Miley 1984; Joly 1991), or that the continuum incident on the broad emission-line gas is different from that observed.

(b) In AGN’s UV-optical spectra there are several clear, related trends: increasing broad-line Fe II emission corresponds to decreasing width (FWHM) of $H\beta$ from the broad-line region (BLR), and to decreasing line emission from lower velocity, lower density gas – $[O\ III]\ \lambda 5007$ emission from the narrow line region (NLR), and UV line emission from lower velocity gas of the BLR (Boroson & Green 1992; Laor et al. 1997; Lawrence et al. 1997; Brotherton et al. 1997, in preparation). ROSAT, with its high sensitivity to soft X-rays, has played an important role in showing that these trends correspond to increasing steepness of the soft X-ray spectra (Boller et al. 1996, Laor et al. 1997, Grupe et al. 1997, in preparation). Correlation analyses show that the dominant spectrum-to-spectrum variation in low and high redshift AGN samples can be reduced to a linear combination of these emission line and continuum parameters – the ‘First Principal Component’. This First Principal Component points to a single, as yet

Send offprint requests to: D. Grupe
(dgrupe@xray.mpe.mpg.de)

* Current address: MPE, Giessenbachstr., D-85748 Garching

mysterious, underlying mechanism relating AGN’s ionizing continuum ($\sim 0.01\text{--}0.2$ keV), the optical Fe II emission, and emission from the BLR and NLR.

While rarely discovered in optical surveys, narrow-line Seyfert 1 nuclei (NLSy1s) are found in abundance in soft-X-ray surveys. These AGN, having broad $H\beta$ emission lines with $\text{FWHM} \lesssim 2000$ km s $^{-1}$, and steep, strong, soft-X-ray spectra, lie at the rich-Fe II extreme of the First Principal Component, and so could give us insight into central engine mechanisms.

One hypothesis proposed to explain their strong, often time-variable, soft X-ray emission, their steep X-ray spectra and narrow BLR $H\beta$ emission lines, is that NLSy1s represent unobscured, low-mass AGN (Boller et al. 1996; Grupe 1996; Grupe et al. 1997, 1997, in preparation). Lower mass means lower gas velocities, producing narrower $H\beta$ emission from the BLR. The strong, soft X-ray-emission arises from an unobscured view of the inner regions of a smaller, and therefore hotter, accretion disk. This direct, rather than scattered-light, view of the tiny emission region allows very rapid variability. Further support for this hypothesis is an observed anticorrelation between optical and soft-X-ray spectral indices, and, in the most luminous AGN, an optical continuum slope equal to that expected from optically thick, thermal, disk emission. On this hypothesis, NLSy1s should be unpolarized.

Another hypothesis suggests that NLSy1s are Seyfert 1s viewed pole-on. Kinematic projection of a disk-like BLR results in a narrower radial velocity distribution, and steep X-ray spectra result from a view of the ‘funnel’ of a geometrically thick accretion disk (Madau 1988).

Perhaps some fraction of these NLSy1s are like the archetype of highly polarized QSOs, IRAS 13349+2438 (Wills et al. 1992b, Brandt et al. 1996). The soft X-ray spectrum of this AGN is strong, variable, and steep, with no signs of absorption by neutral gas. In the optical, it shows typical NLSy1 characteristics – narrow $H\beta$ from the BLR, very strong Fe II, and very weak [O III] $\lambda 5007$. In this AGN there are two views to the central continuum source and BLR – one a direct view that is partially obscured by dusty hot gas in the torus, and the other a less obscured, but indirect, view in which the spectrum is scattering-polarized by electrons or dust in the opening cone of the torus. The unusual combination of UV-optical reddening and lack of cold X-ray absorption was presented by Brandt et al. (1996) as evidence for dusty, ionized gas near the nucleus. Discovery of more such objects would allow further optical-UV-X-ray investigation of this newly discovered constituent of AGN gas.

The above pictures for NLSy1s are not mutually exclusive. In axisymmetric Unified Schemes, a low-mass or thick-disk central engine may be surrounded by a dusty nuclear torus. A low-inclination polar view may reveal an unobscured central engine, while a higher inclination line-of-sight may graze the dusty nuclear torus, passing through ionized gas (e.g. IRAS 13349+2438). As dust fur-

ther dims the direct view of the nucleus, the scattered, polarized AGN spectrum becomes more prominent. At even higher inclinations, cold dusty gas blocks the direct view completely, but a few percent of the NLSy1 spectrum could be scattered towards the observer. Even in a high inclination view, low density NLR gas, ionized on kpc scales, may reveal the presence of a buried NLSy1 in total light. The well-known ‘Seyfert 1 nucleus buried within the prototype Seyfert 2’ galaxy NGC 1068, the Rosetta Stone of Unified Schemes (Antonucci & Miller 1985), may be an excellent high-inclination example with the parsec-scale AGN seen only in scattered light – a faint, polarized spectrum with UV-optical continuum, strong Fe II blends, and BLR $H\beta$ intrinsic $\text{FWHM} \sim 2900$ km s $^{-1}$ (Miller et al. 1991), together with a very steep, unabsorbed soft X-ray spectrum ($\alpha_x \sim 2.4$), showing no variability on several-year time-scales (Elvis & Lawrence 1988; Marshall et al. 1993; Smith et al. 1993).

In this paper we have used broad-band polarimetry and spectroscopy of a ROSAT sample of soft-X-ray-selected AGN to relate scattering and absorption in the optical and X-rays, in order to investigate anisotropic emission, kinematics and dusty gas distribution in these special AGN. In Sect. 2 we describe the sample, as well as observations and data reduction for the optical polarimetry, ROSAT X-ray spectroscopy, and optical spectroscopy. Sect. 3 presents the results, including some correlations. Here we provide more detailed information for the highly polarized sources, and collect together comparable X-ray and optical data for the AGN of Goodrich’s (1989) spectropolarimetry study of optically selected NLSy1s. Sect. 4 discusses the absorption and scattering properties of the sample as a whole, and for individual sources, including a comparison with the optically selected NLSy1s. A summary is given in Sect. 5. Appendix A shows our spectra for all the highly polarized sources discussed in this paper.

2. Observations and Data

2.1. The Soft X-ray Sample

The sample of bright, soft-X-ray AGN (Grupe et al. 1997) was selected from the ROSAT All-Sky Survey (RASS, Voges et al. 1993, 1997). This deep survey, using the Position Sensitive Proportional Counter (PSPC, Pfeffermann et al. 1986), was the first to extend to soft-X-ray photon energies ~ 0.1 keV. Our X-ray sample is completely identified, comprising all 95 AGN with RASS PSPC count rates $\gtrsim 0.5$ cts s $^{-1}$, hardness ratio $\text{HR1} \lesssim 0.0$, and $|b| > 20^\circ$. HR1 is defined as the ratio of the difference to the sum of hard and soft counts of the source, where the hard and soft bands are defined between 0.4–2.4 keV and 0.1–0.4 keV. This HR1 limit corresponds to a steep soft X-ray spectrum with $\alpha_x \gtrsim 1.5$ for $N_H \sim 2 \times 10^{20}$ cm $^{-2}$. The bright, soft X-ray selection results in a sample with very little or no neutral hydrogen absorption. The X-ray and optical

properties of the sample were presented and discussed by Grupe (1996) and Grupe et al. (1997, and 1997 in preparation). About half the sample are NLSy1s. The median FWHM for broad $H\beta$ is 2250 km s^{-1} , with a 90-percentile range from $\sim 1300 \text{ km s}^{-1}$ to 4200 km s^{-1} . We restrict the present polarization survey and analysis to the 43 northern sources ($\delta > 0^\circ$).

2.2. Polarimetry Observations

For the soft X-ray sample, linear polarization was measured using a broad-band polarimeter (Breger 1979) on the Struve 2.1-m telescope at McDonald Observatory. The detector was a cooled ($\sim -20\text{C}$) Hamamatsu R943-02 phototube with extended red sensitivity [GaAs(Cs) photocathode] operated in photon-counting mode. A new interface and data acquisition computer resulted in improved noise characteristics with uncertainties consistent with photon statistics. Otherwise, the filters, observational technique (a few 200-second integrations on-source, interleaved with background integrations), calibrations, and reductions were as described by Wills et al. (1992a). All measurements were made with an aperture of projected diameter $7.4''$. We were interested in searching for scattering polarization, so we aimed for 1σ measurement uncertainties $\lesssim 0.4\%$, because interstellar polarization mechanisms may become important at that level, and are then difficult to distinguish from scattering, based on degree of polarization and wavelength-dependence. In some cases where the measurements indicated real polarization we estimated the contribution from Galactic interstellar polarization by measuring the polarization of stars nearby in projection on the sky. In order to probe as long a path length as possible through our galaxy we chose (where possible) bright, blue stars, preferably known to be of early spectral type. Of the 43 northern AGN, 26 were observed by us and data for 17 were taken from the literature.

2.3. X-ray data

The RASS data have been used for the statistical investigation of the soft-X-ray sample, except for well-known AGN. Details of the reductions are given by Grupe (1996) and Grupe et al. (1997). For the 19 well-known sources we retrieved pointed observation data from the ROSAT public archive at MPE Garching. The January 1996 version of the EXSAS package (Zimmermann et al. 1994) was used for data reduction and analysis. The X-ray spectral index α_x ($F_\nu \propto \nu^{-\alpha_x}$, the photon index $\Gamma = 1 + \alpha_x$) was determined in the energy range $0.1 - 2.4 \text{ keV}$ using single power-law fits, assuming neutral absorption given by Milky Way HI 21cm column densities $N_{\text{H,gal}}$ (Dickey & Lockman 1990) with abundances given by Morrison & McCammon (1983). Uncertainties in α_x are typically 0.1 to 0.5, depending on X-ray brightness. Grupe et al. (1997) also made fits to the X-ray spectra with unconstrained

neutral hydrogen column-density N_{H} . Although the latter was rarely significantly different from Galactic values, we measured the difference $\Delta N_{\text{H}} = N_{\text{H}} - N_{\text{H,gal}}$ as a potential indicator of intrinsic neutral hydrogen absorption. For those objects for which no X-ray spectra were readily available, we used the hardness ratios HR1 and HR2 given in the bright source catalogue (Voges et al. 1997). HR2 is like HR1, but with hard and soft bands defined between $0.9-2.0 \text{ keV}$ and $0.5-0.9 \text{ keV}$. The method is to simulate count-rate spectra for a grid of α_x and N_{H} values, using the known instrumental response. From these spectra we calculate HR1 and HR2 for each combination of α_x and N_{H} . Thus we derive the unique combination α_x and N_{H} that reproduce the observed HR1 and HR2. Uncertainties in ΔN_{H} are similar to those in N_{H} determined from the fits with N_{H} unconstrained. The standard deviations for individual values are about $0.8 \times 10^{20} \text{ cm}^{-2}$ and $1.2 \times 10^{20} \text{ cm}^{-2}$ as determined from the median and mean of the distribution of standard deviations given from the fitting.

For the highly polarized AGN for which ROSAT pointed observations were available, the data were analyzed in the same way as for the RASS data.

2.4. Optical Spectroscopy

In general, we used the medium-resolution optical spectra (FWHM $\sim 5\text{\AA}$) from Grupe (1996) and Grupe et al. (1997, in preparation), obtained in March 1994. The highly polarized objects were re-observed, including $H\beta$ and $H\alpha$, in March 1997 with the 2.1m telescope at McDonald Observatory, but with resolution FWHM $\sim 7\text{\AA}$. Spectra for the PG quasars (resolution 3.6\AA FWHM) are from observations with the 2.7-m telescope at McDonald Observatory in February 1996. A spectrum for RE J1034+39 is from Puchnarewicz et al. (1995a), and for CSO 150, from Bade et al. (1995). Except for QSO 1136+579, and the higher redshift AGN RX J1014.0+4619 and RX J1050.9+5527, we were able to find spectra in the literature: MS 0919.3+5133 (Stephens 1989), EXO 1128.1+6908 (Bedford et al. 1988), UM 472 (Salzer et al. 1989), and NGC 4593 (Dietrich et al. 1994).

The emission line measurements and their uncertainties are presented and described in detail by Grupe et al. (1997, in preparation). Some representative 1σ errors are given in later tables. The blended optical FeII emission was measured and subtracted using a IZw 1 template like that used by Boroson & Green (1992). All other measurements were made from these FeII-subtracted spectra. To determine the rest-frame equivalent width of Fe II we measured the flux in the template between rest wavelengths 4250\AA and 5880\AA , after scaling it to match the object spectra, and then divided by the continuum flux density at 5050\AA . In the following, $H\beta$ refers to the whole $H\beta$ line. $H\beta_b$ refers to the broad component of $H\beta$, obtained after subtraction of the narrow component by using the

[O III] λ 5007 velocity profile as a template. This method subtracts as much of the template as possible while still retaining a sensible shape to the peak of $H\beta_b$. For sources where the narrow-line emission dominates we found an [O III]/ $H\beta_{\text{narrow}}$ intensity ratio of about 10, which is not significantly different from the observed median in Seyfert 1s and Seyfert 1.5s (Koski 1978; Cohen 1983), providing support for our method.

To determine the $H\alpha/H\beta$ intensity ratio, we used the total flux in the lines, because the broad and narrow components are difficult to separate for the $H\alpha$ blend. In general, to subtract the fluxes of the [N II] $\lambda\lambda$ 6548,6584 lines from the $H\alpha$ blend, it was quite adequate to subtract 35% of the [O III] λ 5007 line flux from it (Ferland & Osterbrock 1986). For the highly polarized sources, as we see later, reddening of the NLR emission could be important. So for these we used velocity templates derived from [O III] and total $H\beta$ lines to disentangle the $H\alpha$ -[N II] blend.

Optical continuum spectral indices α_{opt} were measured between rest-frame wavelengths of 4400Å and 7000Å.

2.5. The Optically Selected Sample

For comparison with our soft-X-ray-selected sample, we have compiled polarization, spectroscopic and X-ray data for the optically selected sample of NLSy1s that Goodrich (1989) investigated by spectropolarimetry. While the selection of that sample is based on a mixture of spectroscopic criteria (narrow $H\beta$ emission, strong Fe II emission, [O III] λ 5007/ $H\beta$ < 3, and presence of high-ionization lines) it is unbiased with respect to soft-X-ray properties (α_x or ΔN_H). Measurements were made, as far as possible, in the same way as for our sample. Emission-line measurements were derived from literature data, except for the more highly polarized sources for which we obtained new spectroscopic data including both the $H\beta$ and $H\alpha$ regions (Appendix A).

3. Results

3.1. The ROSAT Soft X-ray AGN Sample

The polarimetry data are given in Table 1, where we list the object's RXJ name derived from the RASS J2000 coordinates, other name, the filter used, degree of polarization p%, and the polarization position angle (E vector, measured on the sky plane in degrees from north through east), and a literature reference where relevant. Errors in p% are 1σ , based on photon-counting statistics. The corresponding position-angle error may be estimated from $28.65^\circ \times$ the fractional error in p%. No corrections have been applied for positive bias in p%. Neither have we made any attempt to correct for unpolarized starlight from the host galaxy. Table 2 gives measurements we made for interstellar polarization. In no case was this large enough to justify a correction to our AGN polarizations.

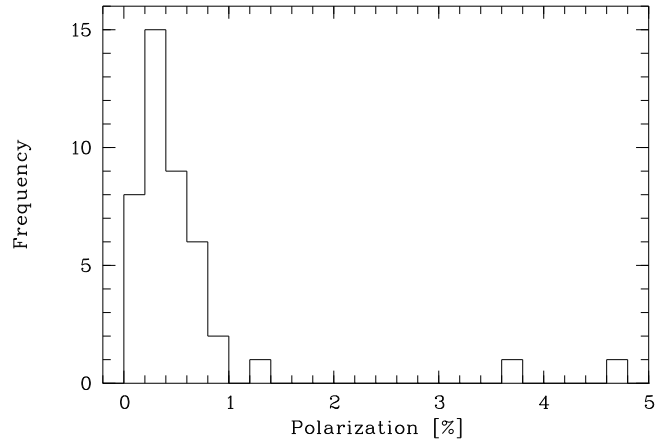


Fig. 1. Distribution of the polarization of the 43 northern soft-X-ray AGN.

Figure 1 displays the distribution of the polarization. Most of the soft-X-ray AGN are of low polarization ($\lesssim 1\%$). Three of the 43 objects show $p > 1\%$. While we have chosen 1% as a practical cut-off for investigating scattered-light polarization, we note that two other AGN, with detailed results from the literature, show low but significant polarization, above interstellar levels. One is the well-known NLSy1 NGC 4051. The other is the broad-lined NGC 5548, with $HR1 \sim 0$.

Because one motivation of this study was to investigate Unified Schemes for NLSy1s, we ask whether there are systematic differences between high and low polarization AGN. The $\text{FWHM}(H\beta_b)$ of the highly polarized AGN are not extremely narrow but typical for the soft X-ray sample. Also, $\alpha_x \sim 1.7$ for the highly polarized AGN, so their soft X-ray spectra tend to be flat compared with most of our sample; but steep compared with ROSAT spectra of optically-selected Seyfert 1 nuclei, for which $\alpha_x \sim 1.0 - 1.7$ (Grupe et al. 1997).

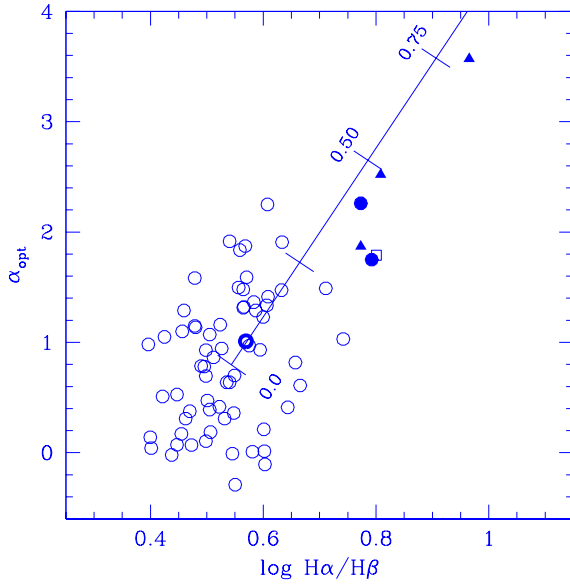
Reddening of the broad lines and continuum is another test for whether we have a direct view to a bare nucleus, with the narrow $H\beta_b$ and steep α_x being intrinsic properties, or whether soft-X-ray-selected AGN with narrow $H\beta_b$ may be viewed through dusty gas near the nucleus, as in orientation Unified Schemes. In Fig. 2 we compare α_{opt} and the Balmer decrement, as indicators of reddening. The low polarization AGN (most of the open circles) have small $H\alpha/H\beta$ ratios, and flat optical spectra (small α_{opt}), and show no relation between $H\alpha/H\beta$ and α_{opt} outside the expected relation resulting from systematic calibration uncertainties, so reddening is unlikely to be important for them. While the low polarization sources do not show significant reddening, the highly polarized sources do. All the polarized AGN (filled symbols) have Balmer decrements $\gtrsim 6$ (except CBS 126, which we discuss later). The one low polarization source with Balmer decrement > 5.8 is IC 3599, which is thought to be a Seyfert 2,

Table 1. Polarimetry of Soft X-ray-selected AGN.

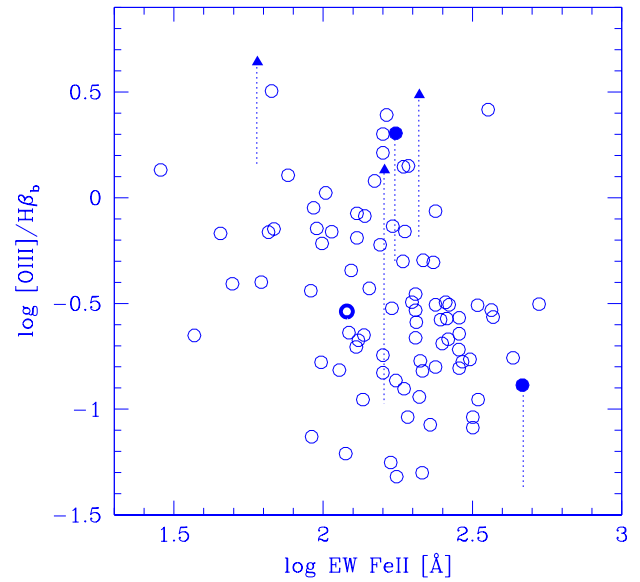
Object RX J	Other Name	Filter	Polarization		Source of Polarimetry data
			p%	Angle (°)	
0922.8+5121	MS 0919.3+5133	none	0.75±0.46	27	McD2.1 March 1997
0925.2+5217	Mkn 110	none	0.21±0.13	—	Berriman et al. (1990)
0956.8+4115	PG 0953+414	none	0.25±0.22	—	Berriman et al. (1990)
1004.0+2855	PG 1001+292	none	0.77±0.22	—	Berriman et al. (1990)
1005.7+4332		none	0.40±0.23	131	McD2.1 April 1996
1013.0+3551	CBS 126	none	1.26±0.13	112	McD2.1 April 1996
		CuSO4	1.19±0.12	118	McD2.1 April 1996
1014.0+4619		none	0.03±0.31	177	McD2.1 April 1996
1017.3+2914		none	0.42±0.16	161	McD2.1 April 1996
1019.2+6358	Mkn 141	3800 - 5600 Å	0.08±0.28	—	Berriman (1989)
		3800 - 5600 Å	0.29±0.28	—	Martin et al. (1983)
1025.5+5140	Mkn 142	none	0.11±0.27	—	Berriman et al. (1990)
1034.6+3938	RE J1034+39	none	0.15±0.21	17	McD2.1 March 1997
		3900 - 5600 Å	0.36±0.13	78	Breeveld & Puchnarewicz (1997)
		5800 - 9200 Å	0.40±0.13	71	Breeveld & Puchnarewicz (1997)
1050.9+5527		none	0.31±0.27	64	McD2.1 April 1996
1058.5+6016	EXO 1055+60	none	0.44±0.26	126	McD2.1 April 1996
1107.2+1628	PKS 1104+16	none	0.63±0.14	157	Wills et al. (1992a)
1117.1+6522		none	0.40±0.22	17	McD2.1 April 1996
1118.5+4025	PG 1115+407	none	0.37±0.24	—	Berriman et al. (1990)
1119.1+2119	Ton 1388	none	0.23±0.11	—	Berriman et al. (1990)
1121.7+1144	Mkn 734	3800 - 5600 Å	0.32±0.13	—	Berriman (1989), Martin et al. (1983)
		none	0.39±0.17	—	Berriman et al. (1990)
1131.1+6851	EXO 1128.1+6908	none	0.29±0.18	37	McD2.1 March 1997
1138.8+5742	QSO 1136+579	none	0.33±0.28	—	McD2.1 March 1997
1139.2+3355	Z 1139+34	none	0.48±0.16	149	McD2.1 April 1996
1145.1+3047	CSO 109	none	0.03±0.19	172	McD2.1 April 1996
1203.1+4432	NGC 4051	3800 - 5600 Å	0.66±0.10	—	Berriman (1989), Martin et al. (1983)
1203.5+0229	UM 472	none	0.62±0.42	41	McD2.1 March 1997
1214.3+1403	PG 1211+143	none	0.07±0.09	—	Berriman et al. (1990)
1231.6+7044		none	0.86±0.23	170	McD2.1 April 1996
1233.6+3101	CSO 150	none	0.20±0.26	175	McD2.1 March 1997
1237.7+2642	IC 3599	none	0.24±0.33	17	McD2.1 April 1996
1239.6−0520	NGC 4593	3800 - 5600 Å	0.49±0.16	—	Berriman (1989), Martin et al. (1983)
1242.1+3317	IRAS F12397+3333	none	3.77±0.20	79.6	McD2.1 April 1996
		U	7.00±0.57	82.1	McD2.1 April 1996
		CuSO4	5.20±0.27	80	McD2.1 April 1996
		B	4.99±0.38	81	McD2.1 April 1996
		V	3.98±0.30	78.7	McD2.1 April 1996
		R	3.50±0.23	80.9	McD2.1 April 1996
		I	2.16±0.33	84.4	McD2.1 April 1996
1312.9+2628		none	0.20±0.29	103	McD2.1 April 1996
1314.3+3429		none	0.30±0.15	88	McD2.1 February 1995
1323.8+6541	PG 1322+659	none	0.81±0.22	—	Berriman et al. (1990)
1337.3+2423	IRAS 13349+2438	none	4.63±0.08	124.5	Wills et al. (1992b)
1355.2+5612		none	0.53±0.22	86	McD2.1 April 1996
1405.2+2555	PG 1402+261	none	0.29±0.14	—	Berriman et al. (1990)
1413.6+7029		none	0.20±0.45	133	McD2.1 April 1996
1417.9+2508	NGC 5548	3800 - 5600 Å	0.71±0.10	—	Berriman (1989), Martin et al. (1983)
1431.0+2817	Mkn 684	none	0.18±0.04	86	Goodrich (1989)
1442.1+3526	Mkn 478	3800 - 5600 Å	0.43±0.15	—	Berriman (1989)
		3800 - 5600 Å	0.46±0.15	—	Martin et al. (1983)
		none	0.26±0.17	—	Berriman et al. (1990)
1618.1+3619		none	0.35±0.35	22	McD2.1 February 1995
1627.9+5522	PG 1626+554	none	0.59±0.19	—	Berriman et al. (1990)
1646.4+3929		none	0.39±0.26	0	McD2.1 April 1996

Table 2. Measurements for interstellar polarization. Right ascension and declination offsets $\Delta\alpha$ and $\Delta\delta$ in arcminutes relative to the AGN coordinates

AGN Name	Star Name	$\Delta\alpha$	$\Delta\delta$	Filter	Polarization %	Angle
CBS 126	SAO 61959	+37.4	-41.8	none	0.10 ± 0.03	177
	Star nf	+0.8	+0.3	none	0.10 ± 0.09	7
RX J1231+70	SAO 07580	+1.3	+86.5	none	0.11 ± 0.05	55
IRAS F12397+3333	SAO 63174	+33.0	+141.6	none	0.04 ± 0.06	12
	SAO 63318	+271.2	-136.1	V	0.03 ± 0.03	126
				R	0.06 ± 0.02	153
				I	0.09 ± 0.02	20

**Fig. 2.** The optical spectral index α_{opt} vs. total $\text{H}\alpha/\text{H}\beta$. Data for our northern and southern X-ray-selected samples are shown as circles, with IC 3599 shown as an open square. See Table 4 for representative 1σ uncertainties. The majority, thought to be unreddened, are shown as open circles. The highly polarized AGN ($p > 1\%$) are shown as filled symbols – circles for the soft-X-ray AGN, triangles for the optically-selected sample. CBS 126, with $p \sim 1\%$, is shown as a heavy circle. The tick-marked line in the plot displays values of $E_{\text{B-V}}$ for equal line and continuum reddening. Polarization data are not available for the majority of southern sources.

or more likely, a starburst nucleus (Sect. 4.4) and therefore different from the rest of our sample. Another test is to look for intrinsic absorption ΔN_{H} in the X-ray spectra. As remarked before, RASS data did not show significant absorption in soft X-rays for any AGN, except IC 3599. However, for some of the highly polarized AGN the higher signal-to-noise pointed observations do show probable absorption (Sect. 3.3)

**Fig. 3.** Line ratio $[\text{O III}]/\text{H}\beta_{\text{b}}$ vs. equivalent width of the optical Fe II blend. See Table 4 for representative 1σ uncertainties. The symbols are as defined in Fig. 2. The dotted vertical lines show the de-reddening paths, based on $E(\text{B-V})$ values derived from Fig. 2.

We can also test how the highly polarized sources might be related to the First Principal Component. In Fig. 3 we show the line ratio $[\text{O III}]/\text{H}\beta_{\text{b}}$ vs. equivalent width of the optical Fe II blend, $\text{EW}(\text{Fe II})$. The low polarization sources of the present sample show the well known inverse $[\text{O III}] - \text{Fe II}$ trend seen for radio-quiet AGN as a whole (Boroson & Green 1992, Grupe et al. 1997, in preparation). Our high polarization sources appear to lie at larger $[\text{O III}]/\text{H}\beta_{\text{b}}$ or larger $\text{EW}(\text{Fe II})$ than the low polarization sources (see Sect. 4).

Table 3. Properties of Goodrich’s optically selected NLSy1 sample

Common Name	RX J ⁱ	Polarization %	Angle	CR ⁱ cts s ⁻¹	HR1 ⁱ	α_x ⁱ	ΔN_H ⁱ 10 ²⁰ cm ⁻²	FWHM(H β_b) ⁱⁱ km s ⁻¹	$\frac{[\text{O III}]}{\text{H}\beta_b}$ ⁱⁱ
Mkn 957	0041.9+4021	0.62±0.06	43	0.09	+0.62	1.5 (a)	+0.0 (a)	685 (a)	0.40 (a)
Mkn 359	0127.5+1910	0.46±0.02	112	0.61	+0.49	1.4 (b)	+0.3 (b)	1350 (b)	1.73 (a)
Mkn 1044	0230.0-0859	0.52±0.05	144	2.14	-0.06	2.0 (b)	+1.1 (b)	1500 (c)	0.22 (a)
Mkn 1239	0952.3-0136	3.35±0.02	130	0.05	+0.81	2.9 (b)	+4.4 (b)	1050 (d)	2.57 (d)
PG 1016+336	1019.1+3322	0.20±0.09	75	—	—	—	—	1310 (a)	0.10 (a)
Mkn 42	1153.7+4612	0.37±0.11	36	0.19	-0.15	1.6 (b)	+0.6 (b)	670 (e)	0.35 (a)
Mkn 766	1218.4+2948	2.34±0.02	90	4.71	-0.02	1.5 (b)	+0.4 (b)	1360 (d)	3.82 (d)
NGC 4748	1252.2-1324	0.12±0.04	83	0.97	+0.20	1.5 (a)	+0.0 (a)	1470 (a)	1.60 (a)
Mkn 783	1302.9+1624	0.25±0.07	2	0.29	+0.88	1.3 (a)	+2.8 (a)	1900 (e)	9.42 (a)
Mkn 684	1431.0+2817	0.18±0.04	86	0.58	-0.23	1.5 (c)	+0.4 (c)	1690 (f)	0.16 (f)
IRAS 15091-2107	1511.9-2119	4.61±0.03	62	0.37	+0.96	1.6 (d)	+26.1 (d)	2250 (d)	1.16 (d)
Mkn 291	1555.1+1911	0.23±0.06	131	—	—	1.1 (b)	-1.4 (b)	700 (g)	0.98 (a)
Mkn 493	1559.1+3501	0.26±0.07	87	0.52	-0.24	1.7 (b)	+0.6 (b)	1360 (d)	0.35 (d)
VII Zw 742	1747.0+6836	0.20±0.10	84	0.21	+0.25	1.3 (a)	-1.2 (a)	1260 (a)	0.53 (a)
Mkn 507	1748.6+6842	0.61±0.03	12	—	—	0.6 (b)	+0.5 (b)	965 (a)	0.73 (a)
Akn 564	2242.6+2943	0.40±0.02	90	0.38	+0.42	2.4 (b)	+1.2 (b)	1000 (b)	1.10 (a)
Mkn 1126	2300.8-1255	0.47±0.04	173	0.35	+0.14	1.5 (a)	-0.2 (a)	2500 (e)	4.15 (a)

ⁱ X-ray data sources:

The count rates CR, and HR1 are from the RASS Bright Source Catalog (Voges et al. 1997). All α_x are from single power law fits with N_H unconstrained. For those objects for which no entry was found, the RX J coordinates were taken from accurate optical positions.

(a) derived from HR1 and HR2 (see Sect. 2.3)

(b) Boller et al. (1996)

(c) RASS observation (Grupe et al. 1997)

(d) ROSAT pointed observation retrieved from the archive

ⁱⁱ Optical data sources:

(a) Goodrich (1989)

(b) Osterbrock & Shuder (1982)

(c) Rafanelli (1985)

(d) McD2.1 March 1997 (see Appendix A)

(e) Osterbrock & Pogge (1985)

(f) McD2.1 March 1994 (Grupe et al. 1997, in preparation)

(g) Lipari et al. (1993)

3.2. Comparison with an Optically Selected NLSy1 Sample

The data for the optically selected NLSy1 sample are presented in Table 3 where we list the object’s common and RX J name, percentage polarization and angle, X-ray count rates and hardness ratio, α_x , ΔN_H , FWHM(H β_b) and [O III]/H β_b ratio. The polarization data are mean values over the whole observed wavelength range (Goodrich 1989). Because soft-X-ray absorption is more probable in this non-soft-X-ray-selected sample we give the α_x determined from an X-ray spectral fit with N_H unconstrained. Sources of data are given below the table.

As expected, the optical selection criteria for this sample result in narrower H β_b and a wider range of HR1 compared with the X-ray-selected sample. Only half of the optically selected sample have steep $\alpha_x \gtrsim 1.5$.

Out of 17 objects, several are polarized at a low level, but three show continuum $p > 1\%$, even $> 2\%$: Mkn 1239, Mkn 766, and IRAS 15091-2107. As for the highly polarized sources of the soft-X-ray sample, these three have FWHM(H β_b) typical of the unpolarized or low-polarization AGN, but they are among the most reddened and have among the highest [O III]/H β_b ratios (Figs. 2 & 3). Mkn 1239 and IRAS 15091-2107 have the largest HR1

of the sample, apparently the result of soft-X-ray absorption. Mkn 783, while not highly polarized, has a high HR1 and soft X-ray absorption, and the largest [O III]/H β_b .

3.3. The Polarized AGN

Two of the three highly polarized AGN of our sample show high and wavelength-dependent polarization – IRAS F12397+3333 (Was 61, Wasilewski 1983) and IRAS 13349+2438 (Fig. 4). The IRAS 13349+2438 polarization has been the subject of intensive investigation as a result of its membership in a warm IRAS sample (Sect. 1). While it provided motivation for the present survey, its inclusion in our statistical discussion is justified because it was discovered by completely independent techniques and was not appreciated to be a member of our sample until much later. But IRAS F12397+3333 is new. The strong increase of polarization towards shorter wavelengths is a clear indication of the dilution of a scattered light AGN spectrum by a redder unpolarized component – either reddened AGN light or starlight. The other highly polarized source, CBS 126, appears to be in a different category. The polarization is small and not strongly wavelength depen-

Table 4. Properties of the highly polarized AGN. Those of our soft-X-ray sample, together with the median and the 90% ranges for the whole soft X-ray sample are to the left. The numbers involved are given in brackets after the median value. The right side of the table gives the values for Goodrich’s highly polarized NLSy1s. The following properties are tabulated: optical monochromatic luminosity $\log \nu L_V$ in Watts, assuming $H_0 = 75 \text{ km s}^{-1} \text{ Mpc}^{-1}$ and $q_0 = 0.5$; redshift z ; $p\%$; FWHM($H\beta_b$) in km s^{-1} , corrected for instrumental resolution; the intensity ratio $[\text{O III}]/H\beta_b$; $\text{Fe II}/H\beta_b$; rest frame equivalent width $\text{EW}(\text{Fe II})$ in \AA ; the total line flux $H\alpha/H\beta$ ratio; α_{opt} between 4400\AA and 7000\AA ; α_x , the X-ray spectral index with N_{H} unconstrained; ΔN_{H} , the intrinsic soft-X-ray absorption column density in units of 10^{20} cm^{-2} ; $\Delta N_{\text{H,opt}}$ is the intrinsic HI column density calculated from E_{B-V} (units as for ΔN_{H}).

Property	CBS 126	IRAS 1239	IRAS 1334	median	90% range	Mkn 766	Mkn 1239	IRAS 1509
$\log \nu L_V$	37.1	36.7	37.7	37.1 (95)	36.4 - 38.2	36.6	36.6	37.0
z	0.079	0.044	0.107	0.107 (95)	0.04 - 0.34	0.013	0.020	0.044
% Pol	1.26 ± 0.13	3.77 ± 0.20	4.63 ± 0.08	0.34 (43)	< 1%	2.34 ± 0.02	3.35 ± 0.02	4.61 ± 0.03
FWHM $H\beta_b$	2850 ± 200	1900 ± 150	2200 ± 200	2250 (91)	1300 - 4200	1360 ± 150	1050 ± 150	2250 ± 200
$[\text{O III}]/H\beta_b$	0.29 ± 0.04	2.00 ± 0.14	0.13 ± 0.02	0.31 (87)	0.05 - 1.40	4.38 ± 0.20	3.06 ± 0.06	1.38 ± 0.06
$\text{Fe II}/H\beta_b$	1.2 ± 0.1	5.5 ± 0.3	6.5 ± 0.1	4.0 (87)	1.0 - 8.0	4.5 ± 0.1	6.3 ± 1.1	4.4 ± 0.1
EW FeII	120 ± 10	175 ± 25	465 ± 15	195 (89)	100 - 360	60 ± 2	210 ± 10	160 ± 10
$H\alpha/H\beta$	3.7 ± 0.3	5.9 ± 0.4	6.2 ± 0.3	3.7 (70)	2.9 - 4.6	5.9 ± 0.3	6.4 ± 0.4	9.2 ± 0.5
α_{opt}	1.0 ± 0.1	2.3 ± 0.1	1.8 ± 0.2	1.0 (88)	0.1 - 1.8	1.9 ± 0.1	2.5 ± 0.1	3.6 ± 0.1
α_x	$1.6^1 \pm 0.1$	$1.7^2 \pm 0.1$	$1.8^2 \pm 0.1$	1.9 (95)	1.5 - 3.2	$1.7^3 \pm 0.1$	$3.1^2 \pm 0.3$	$1.6^2 \pm 1.0$
ΔN_{H}	$-0.1^1 \pm 0.6$	$+1.2^2 \pm 0.3$	$-0.0^2 \pm 0.0$	-0.1 (95)	-1.2 - +1.0	$1.6^3 \pm 0.4$	$4.6^2 \pm 1.8$	$25.8^2 \pm 4.6$
$\Delta N_{\text{H,opt}}$	3	21	17			17	24	39

X-ray data sources:

¹ RASS, Grupe et al. (1997). α_x assumes $N_{\text{H}} = N_{\text{H,gal}}$

² Pointed observation. Data retrieved from the MPE ROSAT archive

³ Very High State from Molendi & Maccacaro (1994)

dent if at all. Unlike the other polarized AGN, the broad lines and continuum are not significantly reddened, and the larger FWHM($H\beta_b$) is more typical of normal Seyfert 1 nuclei. Possibly the polarization arises from transmission of nuclear light through well-aligned grains. For all these reasons, we exclude this source from detailed discussion. The three optically selected NLSy1s with $p > 2\%$ also show $p\%$ increasing to short wavelengths, which, in these AGN, arises from dust-scattered continuum and broad lines (Goodrich 1989).

Further details of the X-ray and optical properties of the highly polarized AGN are given in Table 4. The AGN are approximately in order of increasing $p\%$ and presumed obscuration. For comparison, in the same table, we include the medians and 90 percentile ranges of all measured quantities for the complete soft-X-ray-selected sample. We give α_x and ΔN_{H} based upon the best available X-ray data. For all but CBS 126 and IRAS 13349+2438, the X-ray fits with N_{H} fixed at $N_{\text{H,gal}}$ were unacceptable, so for these others we have adopted the α_x determined from the power-law fits with N_{H} unconstrained.

All scattering-polarized AGN show α_{opt} and $H\alpha/H\beta$ indicative of reddening by dust (Fig. 2, Table 4), and these two quantities are well correlated. Except for IRAS 13349+2438, the degree of polarization is correlated with reddening, but any such real relation must be complicated by differential reddening of scattered and direct light, different amounts of starlight dilution, and the sen-

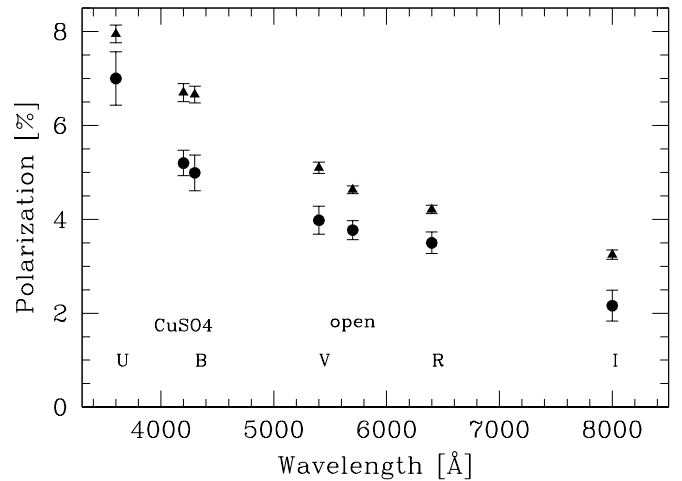


Fig. 4. Wavelength dependence of polarization in IRAS F12397+3333 (circles) and IRAS 13349+2438 (triangles). Wavelengths (\AA) are in the observed frame.

sitivity of polarization to details of the non-spherical, projected geometry. Greater optical reddening appears to be well correlated with stronger cold absorption in soft-X-rays as indicated by ΔN_{H} (Table 4). IRAS 15091–2107, with nearly 3 magnitudes of absorption in the optical, is nearly completely absorbed in soft X-rays below 0.5 keV. We should be careful here. The true soft-X-ray absorption

may be even greater than indicated by ΔN_{H} if a ‘soft excess’ is present at the lowest photon energies – the kind attributed to a very hot accretion disk (Puchnarewicz et al. 1995b; Grupe et al. 1997).

Except for IRAS 13349+2438, the scattering-polarized AGN all have high $[\text{O III}]/\text{H}\beta_{\text{b}}$ ratios (Fig. 3). Alternatively, one could describe the highly polarized sources in this figure as having high $\text{EW}(\text{Fe II})$ for a given $[\text{O III}]/\text{H}\beta_{\text{b}}$ ratio (4.2.1).

Like the X-ray-selected AGN as a whole, the highly polarized AGN show rapid, large-amplitude, time-variability in soft X-rays. IRAS 13349+2438 has shown $\sim 50\%$ variations over ~ 6000 s (Brinkmann et al. 1996, Brandt et al. 1997). For IRAS F12397+3333 we find $\approx 50\%$ variations over ≈ 20 ks. Mkn 766 varied by a factor 2 in 1000 seconds (Leighly et al. 1996). Mkn 1239 varied between the RASS and pointed observations about two years later. The count rate doubled and α_{x} changed from 1.69 during the RASS to 1.94 in the pointed observations, as derived from single power law fits with N_{H} fixed to $N_{\text{H,gal}}$ (Rush & Malkan 1996). IRAS 15091–2107 has shown a probable variation from 0.2 cts s^{-1} to 0.3 cts s^{-1} over 3 days of ROSAT pointed observations, compared with 0.37 cts s^{-1} in the RASS 2.5 years earlier.

4. Discussion

4.1. Statistics of Soft-X-ray NLSy1s

We found 40 of 43 soft-X-ray AGN to have $p < 1\%$, consistent with no intrinsic polarization. Most objects therefore have a direct, unobscured line-of-sight to the nucleus. Some arguments in favor of this can be summarized:

- Lack of cold X-ray absorption along the line-of-sight. The distribution of ΔN_{H} is basically consistent with the errors in N_{H} derived from spectral fits with N_{H} unconstrained (Grupe et al. 1997).
- Rapid X-ray variability is common in this sample, suggesting an emission source less than a few light-days in size (Grupe et al. 1997; see also Boller et al. 1993, 1996, 1997). This argues for a direct view of a tiny powerful nuclear source of X-rays and against an extended source such as is expected for a scattering origin.
- The flat optical spectra and small Balmer line ratios ($\text{H}\alpha/\text{H}\beta$) imply no significant dusty gas.
- The lack of significant optical linear polarization suggests a dustless line-of-sight.

These arguments for a direct unobscured view support the hypothesis, based on spectral energy distributions, that we view the inner accretion disk.

Polarization and reddening are usually associated with cold, dusty gas. What makes our soft-X-ray AGN sample interesting is that these sources have steep X-ray spectra and show no soft X-ray absorption by cold, neutral matter, at least in the RASS spectra (Grupe et al. 1997). Thus, it is a surprise that we find any polarized sources at all –

but we find three – two of which clearly show scattering polarization and signs of UV-optical obscuration. These are not the ones with the narrowest BLR emission lines, or steepest X-ray spectra. Both IRAS F12397+3333 and IRAS 13349+2438 have $\text{FWHM}(\text{H}\beta_{\text{b}})$ close to the ‘magical’ NLSy1 borderline of 2000 km s^{-1} .

4.2. The Polarized AGN

4.2.1. UV-Optical Reddening

Assuming that dust is responsible for the continuum and emission-line reddening in the highly polarized AGN, where is this dust located? The two measures of optical absorption – α_{opt} and $\text{H}\alpha/\text{H}\beta$ – are well correlated (Fig. 2). We show on this figure a line representing equal emission line and continuum reddening with respect to typical, essentially unreddened, values for the X-ray-selected sample as a whole. While we have used total $\text{H}\alpha$ and $\text{H}\beta$ line strengths to determine $\text{H}\alpha/\text{H}\beta$ in this figure, we note that the four most reddened objects have strong narrow line emission. In de-blending the $\text{H}\alpha$ complex, we derived ratios $[\text{N II}] \lambda\lambda 6548, 6584 / [\text{O III}] \lambda 5007$ of 0.4 – 0.6. While uncertain, comparison of these with values in Koski (1978) and Cohen (1983) suggests little reddening of this NLR emission. Less reddening of NLR $\text{H}\alpha$ and $\text{H}\beta$ would imply even larger $\text{H}\alpha_{\text{b}}/\text{H}\beta_{\text{b}}$ ratios for the broad lines than are shown in the figure. Therefore, while the continuum and emission lines appear about equally reddened, it seems likely that the BLR is actually more reddened than the continuum. If more extensive investigation shows this to be true, then the dust may be more closely associated with the BLR than with a region that obscures both the BLR and the continuum source.

A consistency check of BLR reddening is to use the line and continuum reddening determined from the relation shown in Fig. 2 to correct the $\text{H}\beta_{\text{b}}$ intensity, and thus the ratio $[\text{O III}]/\text{H}\beta_{\text{b}}$. If the BLR suffers reddening similar to the continuum, $\text{EW}(\text{Fe II})$ may not be much affected by reddening. This correction brings all the highly polarized sources into line with the low polarization AGN in Fig. 3, consistent with the $[\text{O III}] \lambda 5007$ being relatively unreddened, and arising in a more spatially extended region such as an ionization cone. The BLR reddening has another interesting implication. The highly polarized AGN cover a wide range of $[\text{O III}]/\text{H}\beta_{\text{b}}$ and $\text{EW}(\text{Fe II})$ and, after applying this correction for absorption of $\text{H}\beta_{\text{b}}$ they follow the same well known inverse (‘First Principal Component’) relation between $[\text{O III}]/\text{H}\beta_{\text{b}}$ and $\text{EW}(\text{Fe II})$ shown by other AGN (Boroson & Green 1992; Grupe et al. 1997, in preparation). We note that, for AGN in general, nuclear reddening must contribute to the scatter in the strong $[\text{O III}]/\text{H}\beta_{\text{b}} - \text{EW}(\text{Fe II})$ relation and must partially obscure it in samples unbiased with respect to reddening.

Reddening introduces important biases when QSOs are selected by optical-UV brightness and color. It

is no accident that three IRAS-discovered QSOs are among our sample of highly polarized, reddened AGN. When corrected for reddening IRAS 12397+3333 and IRAS 13349+2438 have $\log \nu L_\nu \sim 38.0$ (watt). Similarly $\log \nu L_\nu$ for Mkn 1239 and IRAS 15091–2107 becomes 37.2 and 38.1. IRAS 12397+3333, IRAS 13349+2438, and IRAS 15091–2107 are then among the most intrinsically luminous AGN at low redshift.

4.2.2. Warm Absorbers

Another way to investigate the dusty regions is to compare the neutral-hydrogen column densities inferred from the intrinsic optical absorption ($\Delta N_{\text{H,opt}}$) and from the soft-X-ray spectral fitting (ΔN_{H}). We derived $E_{\text{B-V}}$ from Fig. 2 to calculate $\Delta N_{\text{H,opt}} \sim k \times E_{\text{B-V}} 10^{20} \text{ cm}^{-2}$ ($k = 49$, Diplas & Savage 1994). The uncertainties could be $\sim 5 \times 10^{20} \text{ cm}^{-2}$, judging by the scatter in Fig. 2. These $\Delta N_{\text{H,opt}}$ values are given in Table 4. It can be seen that the optical reddening significantly overpredicts ΔN_{H} in all cases except perhaps IRAS 15091–2107, where the very high soft X-ray absorption may be consistent with the optical reddening. If we had used $k = 53$ (Predehl & Schmitt 1995; Predehl & Klose 1996) or $k = 66$ (Gorenstein 1975) the discrepancy would have been even greater. It is also probable that less-reddened, scattered light contributes to the optical spectra (Sect. 4.2.3). In this case the true reddening along a direct path to the nucleus, and hence $\Delta N_{\text{H,opt}}$, would be even greater.

The relatively low soft X-ray absorption could be because the X-rays arise in a region more spatially extended than the UV-optical. However, the large amplitude and rapid variability (Sect. 3.3) provides evidence that all or most of the X-ray emission arises within regions light-days to light-months in size. This, together with the high brightness in soft X-rays, argues that we have a direct view to the center in X-rays rather than a view via a parsec-scale scattering region. The relatively low soft X-ray absorption could be because the dust-to-gas ratio is high, or, more likely in this nuclear environment, the dusty gas is at least partially ionized and therefore has greater transparency to soft X-ray photons. The dusty gas is probably related to the ‘warm absorbers’ detected in the O VII and O VIII K-shell edges near 0.7 – 0.8 keV. This ionized gas has now been detected in IRAS 13349+2438 (Sect. 4.2.3), and Mkn 766 (Leighly et al. 1996). Warm absorbers provide a natural tie-in for the UV-optical reddening, X-ray variability, and bright, unabsorbed soft X-ray spectrum. In fact, for IRAS F12397+3333, neutral hydrogen absorption plus a single power-law does not provide a good fit to the X-ray data (Grupe et al. 1997). In the residuals we find a depression near 0.8 keV – an indication of O VII and O VIII absorption edges. The X-ray spectrum and variability will be discussed in more detail together with the results of our spectropolarimetry for this AGN (Wills et al. 1997, in preparation).

Recently, Leighly et al. (1997) show that AGN with warm absorber features in their X-ray spectra tend to be significantly polarized. Related to this, Reynolds (1997) also report that Seyfert 1s with UV absorption also showed X-ray warm absorption.

Walter & Fink (1993) should be given credit for pointing out that some reddened, highly polarized NLSy1s showed anomalously low $\nu F_\nu(1375\text{\AA})$ on a plot of Γ vs. $\nu F_\nu(1375\text{\AA})/\nu F_\nu(2 \text{ keV})$ (their Fig. 8). The low UV flux (by ~ 30) could be explained on the basis of their observed optical reddening, but they found little or no soft X-ray absorption. All except one are NLSy1s, and now known to show warm X-ray absorption. They are IRAS 13349+2438, Mkn 766, NGC 4051 (Table 1, Komossa & Fink 1997), MCG-6-30-15 (FWHM($\text{H}\beta_{\text{b}}$) $\sim 1700 \text{ km s}^{-1}$, Pineda et al. 1980, Reynolds et al. 1997), Akn 564 (Table 3). The other NLSy1s discussed here – IRAS 12397+3333, IRAS 15091–2107, and Mkn 1239 – follow the same trend. When corrected for a reddened continuum all these NLSy1s show the strong increase of Γ with $\nu F_\nu(1375\text{\AA})/\nu F_\nu(2 \text{ keV})$ that led Walter & Fink to argue for a UV to soft X-ray bump in Seyfert 1 nuclei.

4.2.3. Scattered Light Models

We have some evidence that the scattering geometry for NLSy1 may be axisymmetric, and this is certainly true for many other AGN. The polarization (E-vector) is parallel to the major axis of the galaxy in the case of IRAS 13349+2438, and for Mkn 766 and Mkn 1126 the polarization is perpendicular to the elongated radio structure thought to define the jet direction – or angular momentum of the central engine (Ulvestad et al. 1995). Mkn 766 shows an ‘ionization cone’ in the jet direction (Wilson 1997). If we can assume axisymmetry we can relate scattered and direct views to the geometry of the central engine – for example, accretion disk geometry and kinematics.

IRAS 13349+2438 is the best studied of the highly polarized AGN (Wills et al. 1992b; Brandt et al. 1996, 1997; Brinkmann et al. 1996; Hines 1994). In this AGN the contribution of host-galaxy starlight is $< 15\%$, so the wavelength dependence of polarization (Fig. 4) is explained by dilution of polarization by reddened direct AGN light. Therefore we see the AGN from two directions – a direct view, and a view from the vantage point of the scatterers. The polarization E-vector is parallel to the host galaxy’s major axis, suggesting an axisymmetric geometry with obscuring dust in the plane of the galaxy, probably a dusty torus. $\text{H}\beta_{\text{b}}$ and $\text{H}\alpha$ may be slightly narrower in scattered than in total light (Hines 1994). X-ray emission in the ROSAT band is strong and rapidly variable, and therefore not seen reflected from a large (parsec-scale) scattering region, but is instead nuclear light seen directly. The steep X-ray spectrum, lack of neutral absorption in X-rays, but strong UV-optical reddening, led Brandt et al. (1996, 1997) to suggest that ionized, dusty gas absorbs

the nuclear light, thus leading to the first clear detection of warm absorbers in a luminous QSO. Both the fact that the central AGN is still optically visible, and that the absorption is warm, suggest a line-of-sight to the center that grazes the dusty torus: the absorption optical depths are significant but not extremely high; grains are not likely to have formed in the ionized gas, but pre-existing grains could have evaporated from the inner torus on exposure to the nuclear continuum.

A similar scattered-light–dusty torus model is a plausible explanation of our second highly polarized object, IRAS F12397+3333. In this case direct sky survey images show that unpolarized host-galaxy starlight is likely to contribute to the wavelength dependence of $p\%$ (Fig. 4). Warm absorbers provide a natural explanation for the UV-optical reddening, X-ray variability, and bright, essentially unabsorbed soft X-ray spectrum.

Goodrich’s (1989) spectropolarimetry suggests a similar scattering geometry for the three highly polarized AGN in his sample of 17 optically selected NLSy1s (Tables 4 and 3), and our investigation of their UV-optical reddening and X-ray spectra suggest both cold and warm absorbers along a direct path to the nucleus.

The prototypical NLSy1, IZw 1, is an interesting example. Because of its extreme NLSy1 properties, NLSy1 are sometimes called ‘IZw 1’ AGN. It was too weak to be included in our X-ray sample because of anomalously high Galactic HI absorption and variability. Its HR1 was +0.49 during the RASS, but -0.25 during later pointed observations (Boller et al. 1996). It shows significant scattering polarization, with polarized continuum and broad lines (1.7%, Smith et al. 1997) variable in position angle and wavelength-dependence on several-year time scales – maybe shorter – and possibly significant optical reddening, $E(B-V) \sim 0.2$. Its steep soft-X-ray spectrum ($\alpha_x \sim 2.0$) is rapidly variable, with very small intrinsic cold absorption ($1.5 \pm 0.7 \times 10^{20} \text{ cm}^{-2}$). If reddened, this is likely to be another example of a warm absorber – and on axisymmetric Unified Schemes, would therefore be a candidate for a torus-grazing line-of-sight – a potentially powerful illustration that steep X-ray spectra need not be observed from the same direction as the narrow $H\beta_b$ (and other ‘IZw 1’ properties that go along with these properties).

4.2.4. The Nature of NLSy1s

In principle, comparison of scattered and direct views allows a test for the predicted axisymmetry in kinematics, UV- and X-ray emission (Sect.1).

The important conclusion from Goodrich’s (1989) spectropolarimetry is that the narrow $H\beta$ in NLSy1 is more highly polarized than [O III], whose polarization is often unmeasureably small; $H\beta_b$ is narrow not because it arises in the NLR; it is produced in separate, higher density gas.

Assume that polarized $H\beta_b$ represents a scattered light, polar view. Broader polarized $H\beta_b$ than that seen in total light could then be interpreted as evidence for scattering by electrons in hot ionized nuclear gas (Goodrich 1989), or for a dust-scattered view of a high-velocity inner BLR and central continuum source that are obscured in a direct high-inclination, view. Narrower polarized $H\beta_b$ could be interpreted as arising from a polar view of a flattened BLR.

In general, in the ~ 5 cases where a comparison is possible, Goodrich does not find significantly broader $H\beta_b$ in polarized light, and therefore favors scattering by cool dusty gas. This assumes that a predominantly direct view of the center is seen in total light; without knowing $p\%$ for the scattered light alone, we cannot be sure. Also from the similar widths in polarized and total light, we could argue that a higher-velocity, inner BLR is not hidden by the thicker equatorial regions of a dusty torus, and that there is no evidence for an anisotropic velocity field. Mkn 1239 is an interesting exception. Goodrich finds broad, red wings as an additional feature of the $H\beta$ and $H\alpha$ broad lines in polarized flux, which he interprets as arising in a separate electron-scattering region.

AGN like IRAS 13349+2438 and IRAS 12391+3333 of our sample, and three of the Goodrich sample, show significant scattered light views of an optical NLSy1 BLR spectrum ($p_{max} \sim 9, 7, 6, 6, 8\%$), but a direct, higher inclination view of a luminous soft X-ray source with steep 0.2–2 keV spectrum. This rules out the hypothesis in which the narrow $H\beta_b$ and steep α_x belong exclusively to a pole-on view of an optically thick accretion disk with coplanar BLR (e.g., Boller et al. 1996). Mkn 1239 is especially extreme, with $\alpha_x \sim 3$ and $\text{FWHM}(H\beta_b)$ in polarized and total light of $\sim 1500 \text{ km s}^{-1}$ and $\sim 1000 \text{ km s}^{-1}$.

4.3. Unified Schemes

The similarity of the strong, variable, steep X-ray spectra, and narrow $H\beta_b$ in both highly polarized and low polarization AGN support a Unified Scheme in which the low radial BLR velocity dispersion and steep X-ray spectra are intrinsic properties that are not highly anisotropic; the differences are all attributable to orientation-dependent scattering and obscuration. When corrected for optical reddening the highly polarized objects fit the inverse correlation between Fe II and [O III] strengths seen for the unreddened AGN, and even the optically-selected NLSy1s show steep X-ray spectra after correction for cold absorption. The highly polarized AGN lead to a picture of partial obscuration of the central continuum and BLR, with polarized light reaching us from scatterers that have a less-obscured view of the center. While the case for an axisymmetric Unified Scheme is based on polarization alignment in only a few AGN, the partial obscuration of a direct view of the AGN by dusty, ionized gas suggests a line-of-sight grazing the dusty torus. All the above leads us to consider

a unified picture in which all NLSy1s have dusty tori and scatterers, with some lines-of-sight unobscured.

Our sample of 43 comprises all AGN in a ROSAT X-ray source sample, complete to a given X-ray count rate and hardness ratio. All the AGN (except IC 3599) have prominent AGN-like optical continua and broad $H\beta$. There are no classical Seyfert 2s in the sample at all, demonstrating that our view towards their nuclei is opaque in soft X-rays. Our sample includes only two out of 43 AGN that are clearly scattering-polarized, demonstrating that warm, dusty absorbers are rarely found along sight-lines without accompanying cold absorbing gas. In fact, the soft-X-ray absorption seen in the highly polarized AGN of the X-ray and optically selected samples, while small, does correlate well with optical reddening, but we suggest that an additional N_{H} of $1.5 - 2 \times 10^{21} \text{ cm}^{-2}$ is accounted for by warm X-ray absorbers.

Assuming axisymmetry, the low polarization AGN represent unobscured views from within an ionization-scattering cone. Several sources in both samples show observed white light $p < 1\%$. Goodrich (1989) found that some lower polarization objects show $p\%$ increasing to shorter wavelengths with significant continuum and broad-line polarization, indicating that a number of sources in both samples show similar scattering geometry. Their smaller polarizations may arise from a smaller scattering angles, and greater dilution by unpolarized AGN and host-galaxy light. At higher inclination angles, partially ionized dusty gas absorbs the UV, soft X-rays and $\sim 0.7 \text{ keV}$ X-rays. It doesn't take much dusty gas, like that of our interstellar medium, to completely block the UV and soft-X-rays, so it is probably not surprising that only 5% of our sample are highly polarized warm absorbers. As the inclination increases the thicker dusty torus blocks all but the harder X-rays (5-15 keV, e.g. Comastri et al. 1995). At higher inclinations, IRAS 12397+3333, Mkn 766, Mkn 1239, and IRAS 1509-2107 would appear as Seyfert 2s (like NGC 1068, discussed below). Strong-FeII, weak-[O III] AGN like IRAS 13349+2438 would appear as galaxies with weak emission lines, detectable in hard X-rays and warm mid-infrared surveys. Deep X-ray spectral surveys of complete infrared-selected AGN are needed to understand the covering by cold and warm X-ray absorbers.

The archetype buried Seyfert 1 nucleus, revealed in the polarized light spectrum of the classical Seyfert 2, NGC 1068, may simply be a more edge-on view of a NLSy1, with the UV-optical and soft X-rays seen only in scattered light. In this case, a spatially resolved dust-scatterer sees a low inclination view with $\text{FWHM}(H\beta_{\text{b}}) \sim 2900 \text{ km s}^{-1}$, but electron scatterers within a few parsecs of the nucleus produce $\text{FWHM}(H\beta_{\text{b}}) \sim 4480 \text{ km s}^{-1}$ presumably the result of thermal broadening at $\sim 10^6 \text{ K}$ (Miller et al. 1991). Electron-scattering is wavelength independent, so an intrinsic, polar view is seen in soft X-rays, with $\alpha_{\text{x}} \sim 2$ (Marshall et al. 1993; Pier et al. 1994). Unlike the result for most NLSy1s with purported

low-inclination views, the X-ray spectrum shows no time-variability over several years (Smith et al. 1993), consistent with scattering of X-rays from a parsec-scale region.

4.4. IC 3599

IC 3599 is the only AGN of the soft X-ray selected sample to be classified as a Seyfert 2 galaxy (Grupe et al. 1995). Unified Schemes suggest that scattered light polarization might be detectable. We find no significant polarization, but some optical absorption may be present (Fig. 2), a result that may favor the starburst classification suggested by Bade (1993). This object would not usually fit the criteria for inclusion in the soft X-ray sample; it just happened to be in an X-ray outburst at the time of the RASS (Brandt et al. 1995; Grupe et al. 1995).

5. Summary

We have surveyed the optical linear polarization of the 43 northern objects of our completely-identified sample of bright soft-X-ray-selected ROSAT AGN. All except one are Seyfert 1 nuclei, with median $\text{FWHM}(H\beta_{\text{b}})$ of 2250 km s^{-1} . Most (40) are of low polarization with $p < 0.5\% - 1\%$, and have flat blue continua and small Balmer decrements. This supports the suggestion from rapid X-ray variability, disk-like spectral energy distribution, and lack of cold X-ray absorption, that we are viewing a bare AGN disk (Grupe et al. 1997).

Three AGN show significant polarization, with no preference for the narrowest $H\beta_{\text{b}}$ or steepest α_{x} . One, CBS 126, has $p \sim 1.3\%$ with no clear wavelength dependence. Two, IRAS 13349+2438 and IRAS 12397+3333, show high degrees of polarization increasing to short wavelengths, and significant optical reddening. In IRAS 13349+2438 a dusty torus dims the central luminous AGN, revealing a less-reddened polar view of the continuum and BLR in scattered light (Wills et al. 1992b). This partial dust covering forms the basis for Unified Schemes – accounting for very different obscured or unobscured views of the same central engine. Brandt et al. (1996) explained its rapidly-variable and bright X-ray spectrum, lack of soft-X-ray absorption, but reddened UV-optical spectrum, by dusty, ionized gas (warm absorbers) along the line-of-sight to the center. The optical polarization and reddening, together with its rapidly-variable and steep X-ray spectrum, suggest the same scattering-warm-absorber picture for IRAS 12397+3333.

We have compared the polarization, spectroscopic and X-ray properties of our two highly-polarized sources with three discovered by Goodrich (1989) among a heterogeneous sample of 17 optically-selected NLSy1s. Only about half the optically-selected sample have steep α_{x} , $\gtrsim 1.5$. There appear to be correlations among indicators of dust and cold X-ray absorption: $p\%$, α_{opt} , $H\alpha/H\beta$, and ΔN_{H} . When the $H\beta_{\text{b}}$ strength is corrected for reddening, the

highly polarized objects have similar $[\text{O III}]/\text{H}\beta_b$ to the low polarization AGN, and show the same ‘First Principal Component’ $[\text{O III}]/\text{H}\beta_b - \text{EW}(\text{Fe II})$ anticorrelation. However the neutral soft X-ray absorption is overpredicted by the optical reddening by $\sim 5 \times 10^{20} \text{ cm}^{-2}$. So, in line with the warm absorbers seen in IRAS 1334+2438 and Mkn 766, dusty partially ionized gas is almost certainly absorbing nuclear light.

The intrinsic properties of the high and low polarization AGN are similar, including narrow $\text{H}\beta_b$ and steep α_x ; the differences are all attributable to orientation-dependent scattering and obscuration, and this is supported by the periscopic geometry deduced for individual polarized AGN. Thus an orientation Unified Scheme may link all the AGN of our sample, and NLSy1s in general.

Acknowledgements. We gratefully acknowledge Mike Brotherton, Karen Leighly, and the referee for valuable comments that improved the paper. We thank Darrin Crook, Mike Ward, David Doss, Ed Dutchover, Marian Frueh, and Jerry Martin of McDonald Observatory for instrumental and observing help. We also want to thank Norbert Bade (Sternwarte Hamburg), Wolfram Kollatschny (Universitäts-Sternwarte Göttingen), and Liz Puchnarewicz (University College London), for supplying their spectra of CSO 150, NGC 4593, and RE J1034+39; also Laura Kay, Sally Stephens, and Hien Tran, for finding a spectrum for MS 0919.3+5133. We also thank Neil Brandt for sending his preprints on IRAS 13349+2438, and Alice Breeveld for her preprint on RX E1034+39. DG and BJW were supported by a grant from the Space Telescope Science Institute (GO-06766) and NASA Long Term Space Astrophysics grant NAG5-3431. This research has made use of the NASA/IPAC Extragalactic Database (NED) which is operated by the Jet Propulsion Laboratory, California Institute of Technology, under contract with the National Aeronautics and Space Administration.

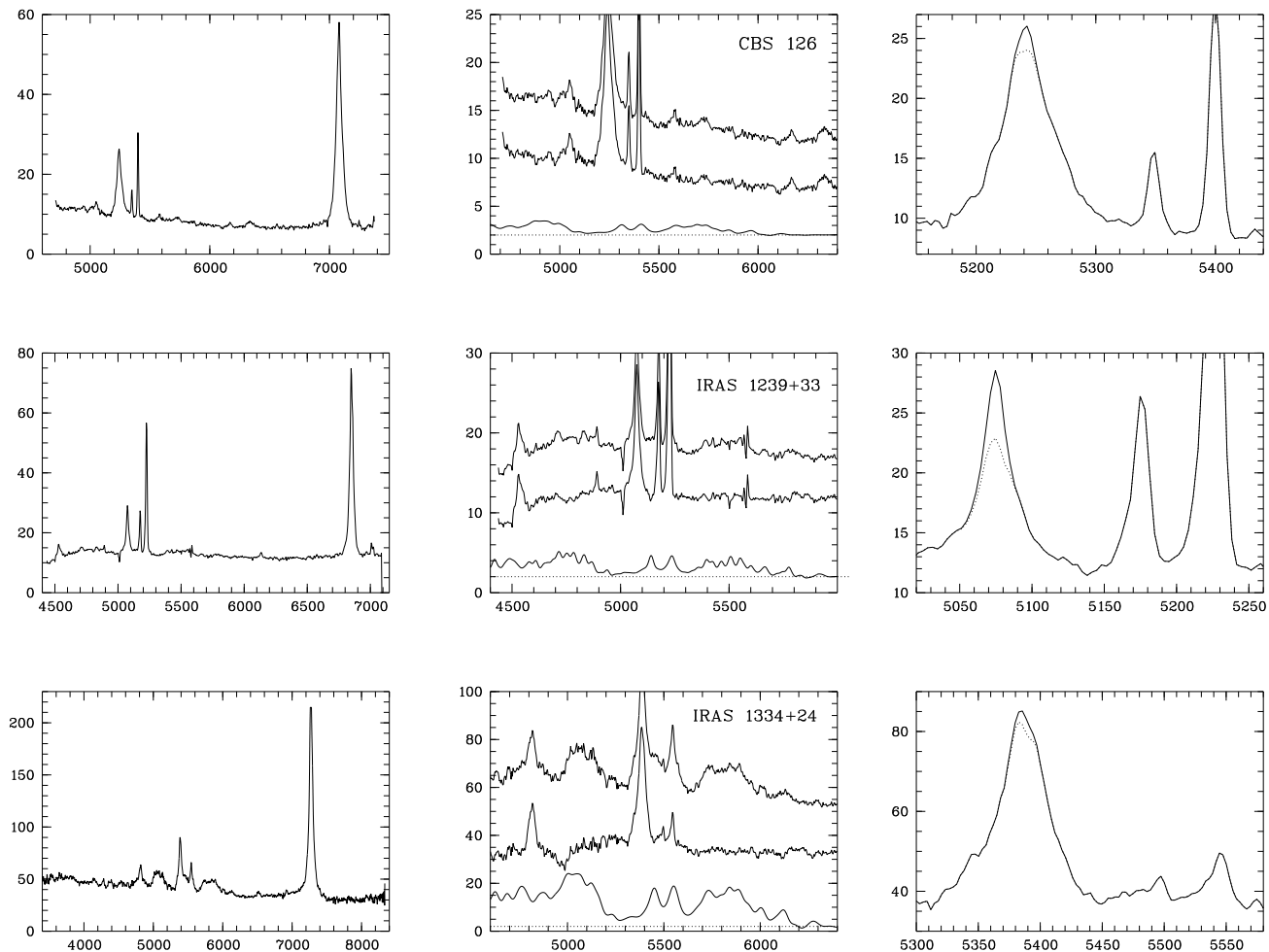
References

- Antonucci R.R.J., Miller J.S., 1985, ApJ 297, 621
 Bade N., 1993, PhD Thesis Universität Hamburg
 Bade N., Fink H.H., Engels D., et al., 1995, A&AS 110, 469
 Bedford D.K., Vilhu O., Petrov P., 1988, MNRAS 234, 319
 Berriman G., 1989, ApJ 345, 713
 Berriman G., Schmidt G.D., West S.C., Stockman H.S., 1990, ApJS 74, 869
 Boller Th., Trümper J., Molendi S., et al., 1993, A&A 279, 53
 Boller Th., Brandt W.N., Fink H.H., 1996, A&A 305, 53
 Boller Th., Brandt W.N., Fabian A.C., Fink H.H., 1997, MNRAS 289, 393
 Boroson T., Green R., 1992, ApJS 80, 109
 Brandt W.N., Pounds K.A., Fink H.H., 1995, MNRAS 273, L47
 Brandt W.N., Fabian A.C., Pounds K.A., 1996, MNRAS 278, 326
 Brandt W.N., Mathur S., Reynolds C.S., Elvis M., 1997, MNRAS (in press)
 Breeveld A.A., Puchnarewicz E.M., 1997, MNRAS (in press)
 Breger M., 1979, ApJ 233, 97
 Brinkmann W., Kawai N., Ogasaka Y., Siebert J., 1996, A&A 316, 9
 Cohen R.D., 1983, ApJ 273, 489
 Collin-Souffrin S., Hameury J.-M., Joly M., 1988, A&A 205, 19
 Comastri A., Setti G., Zamorani G., Hasinger, G., 1995, A&A 296, 1
 Dickey J.M., Lockman F.J., 1990, ARA&A 28, 215
 Dietrich M., Kollatschny W., Alloin D., et al., 1994, A&A 284, 33
 Diplas J.M., Savage B.D., 1994, ApJ 427, 274
 Elvis M., Lawrence A., 1988, ApJ 331, 161
 Ferland G.J., Osterbrock D.E., 1986, ApJ 300, 658
 Goodrich R.W., 1989, ApJ 342, 224
 Gorenstein P., 1975, ApJ 198, 95
 Grupe D., 1996, PhD Thesis, Universität Göttingen
 Grupe D., Beuermann K., Mannheim K., et al., 1995, A&A 299, L5
 Grupe D., Beuermann K., Thomas H.-C., Mannheim K., Fink H.H., 1997, A&A (in press)
 Hines D.C., 1994, PhD thesis, University of Texas at Austin
 Hines D.C., Wills B.J., 1993, ApJ 415, 82
 Joly M., 1991, A&A 242, 49
 Komossa S., Fink H.H., 1997, A&A 322, 719
 Koski A., 1978 ApJ, 223, 56
 Laor A., Fiore F., Elvis M., Wilkes B.J., McDowell J.C., 1997, ApJ 477, 93
 Lawrence A., Elvis M., Wilkes B.J., McHardy I., Brandt W.N., 1997, MNRAS 285, 879
 Leighly K.M., Mushotzky R.F., Yaqoob T., Kunieda H., Edelson R., 1996, ApJ 469, 147
 Leighly K.M., Kay L.E., Wills B.J., Wills D., Grupe D., 1997, ApJ 489, L137
 Lipari S., Terlevich R., Macchetto F., 1993, ApJ 406, 451
 Madau P., 1988, ApJ 327, 116
 Marshall F.E., Netzer H., Arnaud K.A., et al., 1993, ApJ 405, 168
 Martin P.G., Thompson I.B. Maza J., Angel J.R.P., ApJ 266, 470
 Miller J.S., Goodrich R.W., Matthews W.G., 1991, ApJ 378, 47
 Molendi S. Maccacaro T., 1994, A&A 291, 420
 Morrison R., McCammon D., 1983, ApJ 270, 119
 Netzer H., 1985, ApJ 289, 451
 Norman C., Miley G., 1984, A&A 141, 85
 Osterbrock D.E., Shuder J.M., 1982, ApJS 49, 149
 Osterbrock D.E., Pogge R.W., 1985, ApJ 297, 166
 Pfeffermann E., Briel U.G., Hippmann H., et al. 1986, SPIE 733, 519
 Pier E.A., Antonucci R.R.J., Hurt T., Kriss G., Krolik J. 1994, ApJ 428, 124
 Pineda F.J., Delvaille J.P., Schnopper H.W., Grindlay J.E., 1980, ApJ 237, 414
 Predehl P., Schmitt J.H.M.M., 1995, A&A 293, 889
 Predehl P., Klose S., 1996, A&A 306, 283
 Puchnarewicz E.M., Mason K.O., Siemiginowska A., Pounds K.A., 1995a, MNRAS 276, 20
 Puchnarewicz E.M., Branduardi-Raymond G., Mason K.O., Sekiguchi K., 1995b, MNRAS 276, 1281
 Rafanelli P., 1985, A&A 146, 17
 Reynolds C.S., 1997, MNRAS 286, 513

- Reynolds C.S., Ward M.J., Fabian A.C., Celotti A., 1997, MNRAS (in press)
- Rush B., Malkan M.A., 1996, ApJ 456, 466
- Salzer J.J., MacAlpine G.M., Boroson T.A., 1989, ApJS 70, 447
- Smith D.A., Done C., Pounds K.A., 1993, MNRAS 263, 54
- Smith P.S., Schmidt G.D., Allen R.G., Hines D.C., 1997, ApJ 488, 202
- Stephens S.A., 1989 AJ 97, 10
- Ulvestad J.S., Antonucci R.R.J., Goodrich R.W., 1995, AJ 109, 81
- Voges W., 1993, Adv. Space Res. 13, 391
- Voges W., Aschenbach B., Boller Th., et al., 1997, A&AS (in press)
- Walter R., Fink H.H., 1993, A&A 274, 105
- Wasilewski A.J., 1983, ApJ 272, 68
- Wills B.J., Hines D.C., 1997, Clues to Outflows: Polarization of IRAS-Selected QSOs. In: Arav N., Shlosman I., Weymann R.J. (eds.) Mass Ejection from AGN. PASPC 128, 99
- Wills B.J., Wills D., Breger M., Antonucci R.R.J., Barvainis, R. 1992a, ApJ 398, 454
- Wills B.J., Wills D., Evans N.J., et al., 1992b, ApJ 400, 96
- Wilson A.S., 1997, Ap&SS (in press)
- Zimmermann H.U., Becker W., Belloni T., et al., 1994, EXSAS User's Guide, MPE Report 257

A. Optical Spectra

We display the optical spectra of the highly polarized sources of the ROSAT soft-X-ray sample, CBS 126, IRAS F12397+3333, and IRAS 13349+2438, and of Goodrich's sample, Mkn 766, Mkn 1239, and IRAS 15091–2107, in order of increasing $p\%$ and Balmer decrement within each sample, and approximately in order of increasing obscuration as a whole. The left panel shows the whole wavelength range covering $H\beta$ and $H\alpha$. The middle panel illustrates the Fe II blend contribution in the $H\beta$ region: the observed spectrum, (displaced in F_λ), the Fe II-subtracted spectrum (not displaced), and the Fe II template with its zero level shown as a dotted line. The right panel shows the $H\beta$ and $[O III] \lambda 4959,5007$ profiles, illustrating the removal of NLR emission from $H\beta$. All spectra were obtained at the McDonald Observatory at the 2.1m Struve telescope in March 1997, except the spectrum of IRAS 13349+2438, which was obtained at the 2.7m Smith telescope in March 1987 (Wills et al. 1992b). The spectra are plotted as flux density F_λ in units of $10^{-19} \text{ W m}^{-2} \text{ \AA}^{-1}$ vs. λ in \AA . The absolute flux density calibration is uncertain.



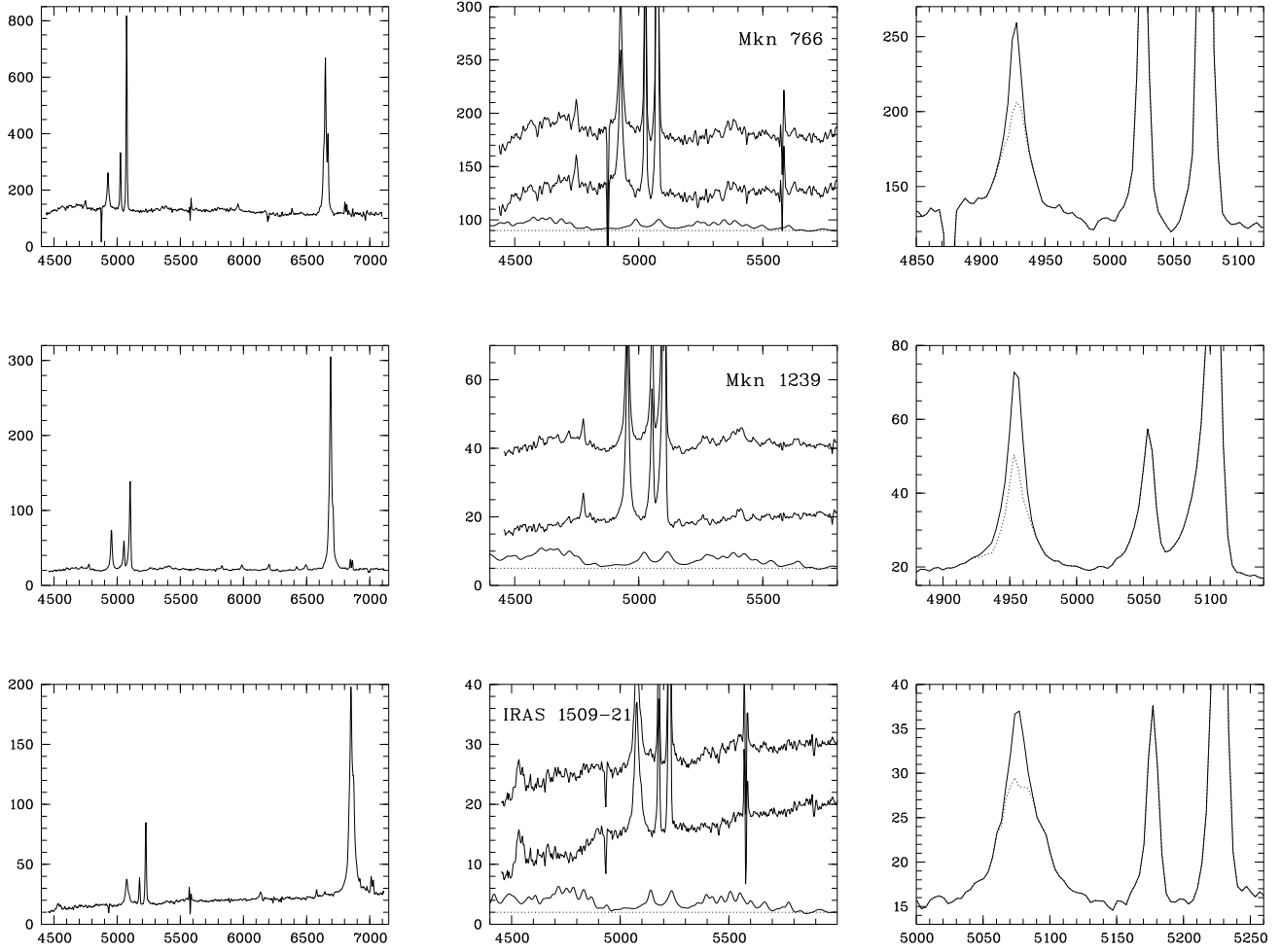


Fig. 5. Optical spectra of the highly polarized AGN